Synthesis and Evaluation in Rats of the Dopamine $D_{2/3}$ Receptor Agonist ^{18}F-AMC20 as a Potential Radioligand for PET

Vladimir Shalgunov[1], Jan-Peter van Wieringen[2], Henk M. Janssen[3], P. Michel Fransen[3], Rudi A.J.O. Dierckx[1], Martin C. Michel[4], Jan Booij[2], and Philip H. Elsinga[1]

[1]Department of Nuclear Medicine and Molecular Imaging, University Medical Center Groningen, University of Groningen, Groningen, The Netherlands; [2]Department of Nuclear Medicine, Academic Medical Center, University of Amsterdam, Amsterdam, The Netherlands; [3]SyMO-Chem BV, Eindhoven, The Netherlands; and [4]Department of Pharmacology, Johannes Gutenberg University, Mainz, Germany

Dopamine $D_{2/3}$ receptor ($D_{2/3}$R) agonist PET tracers are better suited for the imaging of synaptic dopaminergic neurotransmission than $D_{2/3}$R antagonists and may also offer the opportunity to study in vivo the high-affinity state of $D_{2/3}$R ($D_{2/3}$RHigh). With the aim to develop ^{18}F-labeled $D_{2/3}$R agonists suitable for widespread clinical application, we report here on the synthesis and in vitro and in vivo evaluation of a $D_{2/3}$R agonist ligand from the aminomethyl chromane (AMC) class—(*R*)-2-[(4-^{18}F-fluorobenzylamino)methyl]chroman-7-ol (^{18}F-**AMC20**). **Methods:** In vitro affinities of **AMC20** toward dopaminergic receptor subtypes were measured in membrane homogenates prepared from HEK293 cells expressing human dopamine receptors. Agonism of **AMC20** was assessed in the arrestin recruitment assay in Chinese hamster ovary–K_1 cells expressing the long isoform of D_2R (D_2RLong). $D_{2/3}$R-specific binding of ^{18}F-**AMC20** was evaluated in brain slices of Sprague–Dawley rats by in vitro autoradiography and in living rats by in vivo small-animal PET imaging and ex vivo autoradiography. PET data were analyzed with 1- and 2-tissue compartmental models, the simplified reference tissue model, and Logan graphical analysis. Specificity of binding was tested by blocking $D_{2/3}$R with raclopride (coincubation with 10 μM in vitro, administration of 1.0 mg/kg in vivo). **Results:** In membrane homogenates, **AMC20** demonstrated picomolar affinity at D_2RHigh (mean inhibition constant [K_i] = 85 pM) and excellent selectivity against the low-affinity state of D_2R (D_2RLow) (mean K_i = 84 nM, 988-fold selectivity) and D_1-like receptors (mean K_i = 5,062 nM at D_1R). The efficacy of **AMC20** was 90% of that of dopamine in the arrestin recruitment assay. Up to 70% of total binding of ^{18}F-**AMC20** in the $D_{2/3}$R-rich striatum in rat brain slices was $D_{2/3}$R-specific; in living rats, the uptake ratio between the striatum and the $D_{2/3}$R-poor cerebellum reached 2.0–2.5, depending on the measurement method. Radiometabolites of ^{18}F-**AMC20** did not enter the brain. Striatal binding potential of ^{18}F-**AMC20** varied between 0.49 and 0.59 depending on the estimation method. Pretreatment with 1 mg of raclopride per kilogram reduced the apparent specific binding of ^{18}F-**AMC20** in the striatum. **Conclusion:** ^{18}F-**AMC20** shows specific binding to $D_{2/3}$R in the striatum of living rats. Further optimization of the chemical structure of ^{18}F-**AMC20** can lead to ^{18}F-labeled $D_{2/3}$ agonist PET tracers more suitable for in vivo clinical application.

Received Jul. 10, 2014; revision accepted Nov. 6, 2014.

For correspondence or reprints contact: Philip H. Elsinga, Department of Nuclear Medicine and Molecular Imaging, University Medical Center Groningen, Hanzeplein 1, 9713 GZ Groningen, The Netherlands.

E-mail: p.h.elsinga@umcg.nl

Published online Dec. 4, 2014.

Key Words: agonist tracer; dopamine receptor; PET; ^{18}F

J Nucl Med 2015; 56:133–139
DOI: 10.2967/jnumed.114.145466

Imaging of dopamine D_2 and D_3 receptors ($D_{2/3}$R) by PET is a topic of particular interest, because deregulation of $D_{2/3}$ signaling is implied in many neuropsychiatric disorders (*1–4*).

Most PET tracers currently used for $D_{2/3}$R imaging are antagonists (*5*). Throughout the recent 2 decades, development of agonist tracers for G-protein–coupled neurotransmitter receptors has gained popularity, spurred by the consistent observations by several authors (*6–8*) that in vitro agonists bound to receptor–G-protein complexes with higher affinity than to free receptors, whereas antagonists bound to all receptors with equal affinity.

Preference for this subset of receptors (called the high-affinity state) makes agonists potentially better suited than antagonists for the imaging of synaptic neurotransmission, because the neurotransmitters themselves are agonists and exhibit the same preference. Indeed, ^{11}C-labeled $D_{2/3}$R agonists demonstrated greater sensitivity to amphetamine-induced dopamine release in humans than the antagonist ^{11}C-raclopride (*9,10*).

Moreover, dysregulated relative abundance of the high-affinity state of $D_{2/3}$R might underlie the state of dopamine supersensitivity, which is associated with psychosis, Parkinson disease, and addiction (*11*). Agonist tracers might provide new insights for the research into and (early) diagnosis of such disorders.

Of many candidate compounds of various classes tested as potential $D_{2/3}$R agonist PET tracers (*12*), only 3 were eventually used in humans, namely the apomorphines (–)-*N*-propyl-norapomorphine (^{11}C-(–)**NPA**) and (*R*)-2-$^{11}CH_3$O-*N*-*n*-propylnorapomorphine (^{11}C-**MNPA**) and the naphtoxazine (+)-4-propyl-3,4,4a,5,6,10b-hexahydro-2H-naphtho[1,2-b][1,4]oxazin-9-ol (^{11}C-(+)**PHNO**). The scope of use of ^{11}C tracers is limited by the short half-life of ^{11}C (20.4 min), whereas tracers labeled with longer-living radioisotopes such as ^{18}F (half-life, 109.8 min) have a much greater potential. (*R*)-(−)-2-^{18}F-fluoroethoxy-*N*-*n*-propylnorapomorphine (^{18}F-**MCL-524**), an ^{18}F-labeled apomorphine derivative, showed promising results in monkeys (*13*) but has not yet been reported to be used in humans.

We aimed to develop ^{18}F-labeled $D_{2/3}R$ agonist radioligands for PET. We have based our research on the aminomethyl chromanes (AMCs), a class of $D_{2/3}$ agonists first described as such by Mewshaw et al. (*14*). Until now, AMCs have not been used for PET tracer development.

Elaborating on the molecules described by Mewshaw, in particular (*R*)-2-(benzylaminomethyl)chroman-7-ol **(AMC1),** we have recently prepared a series of fluorinated AMCs and evaluated them as potential PET tracers (*15*). By attaching a fluoroalkoxy moiety to the benzyl ring of **AMC1** and systematically varying the length of the fluoroalkoxy group, we obtained **FBu-AMC13** and **FEt-AMC13** (Fig. 1). ^{18}F-**FEt-AMC13** demonstrated specific binding to striatal $D_{2/3}R$ in rat brain slices and in living rats, with a strong preference toward $D_{2/3}$RHigh (high-affinity state of $D_{2/3}R$) (*16*).

The ^{18}F-fluorine label can also be attached directly to the benzyl ring of **AMC1**, minimizing the alteration of the **AMC1** structure caused by the introduction of the label and providing greater potential in vivo stability than ^{18}F-fluoroalkyl derivatives. In fact, a racemic para-fluorobenzyl derivative of **AMC1** was already reported by Mewshaw to have subnanomolar affinity toward D_2RHigh receptors and good selectivity against D_2RLow (low-affinity state of D_2R) (*1*). Here we report the preparation of the R enantiomer of this derivative, **AMC20,** and its in vitro and in vivo evaluation.

MATERIALS AND METHODS

Chemistry, Radiochemistry, and Pharmacology

The preparation and characterization of ^{18}F-**AMC20** and of its ^{19}F reference and precursors are described in the supplemental materials (available at http://jnm.snmjournals.org).

In vitro binding experiments in HEK293 cell membrane homogenates were performed as described earlier (*15*). The β-arrestin recruitment assay was performed as described in the supplemental materials.

In vitro autoradiography in rat brain slices is described in detail in the supplemental materials. Briefly, sagittal slices from male Sprague–Dawley rats (Harlan) containing both striatum and cerebellum were incubated in a Tris-based buffer (pH 7.4) in the presence of varying concentrations of ^{18}F-**AMC20** (~2–80 nM) with or without 10 μM raclopride ($D_{2/3}$ antagonist) or 100 μM guanosine-5′-triphosphate sodium salt (GTP, stimulator of G-protein uncoupling from the receptors). Then the slices were washed, dried, and exposed against phosphor storage screens. On the resulting images, striatal and cerebellar regions of interest (ROIs) were manually drawn, and mean exposure per region was quantified.

Animals

Animal experiments were performed by licensed investigators in compliance with the Law on Animal Experiments of The Netherlands. The protocol was approved by the Committee on Animal Ethics of the University of Groningen. Young male (age, 10–12 wk; body weight, 300–350 g) Sprague–Dawley rats were used for all experiments. The rats were maintained on a 12-h light/12-h dark regime and were fed standard laboratory chow ad libitum.

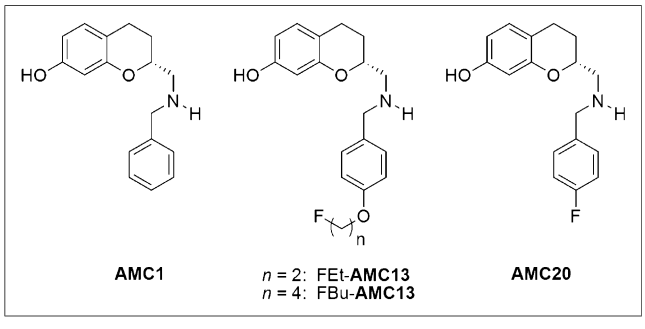

FIGURE 1. Structures of **AMC1, FBu-AMC13, FEt-AMC13,** and **AMC20.**

Small-Animal PET

The distribution of ^{18}F-**AMC20** was studied in rats pretreated with physiologic saline (controls, $n = 4$) or the $D_{2/3}R$ antagonist raclopride (1 mg/kg) (as tartrate salt, $n = 4$). Saline and raclopride (in random order) were injected intravenously about 30 min before tracer injection. An extra group of rats ($n = 4$) was pretreated with saline and injected with ^{11}C-raclopride to serve as positive controls for $D_{2/3}$-specific brain uptake.

Before all manipulations, the animals were anesthetized with a mixture of isoflurane/air (inhalation anesthesia, 5% ratio during induction, 2% at maintenance). Cannulae were inserted into their left femoral arteries and veins; the operation took 45–50 min. Then the rats were positioned supine inside the camera (Focus 220 microPET; Siemens-Concorde), 2 at a time, one above the other with their heads in the camera's field of view. A 515-s transmission scan with a ^{57}Co point source was obtained. Tracer (^{18}F-**AMC20** or ^{11}C-raclopride, Table 1) in 1 mL of saline was injected through the venous cannula as a 60-s-long bolus using an infusion pump. The second (upper) animal was injected 16 min after the first (lower).

PET data were acquired using a list-mode protocol (106 min for ^{18}F-**AMC20,** 76 min for ^{11}C-raclopride). Acquisition began at the moment of the injection of radioactivity in the first rat.

In each rat, arterial blood samples of 0.10–0.15 mL were withdrawn through the arterial cannula at 10, 20, 30, 40, 50, 60, 90, 120, 180, 300, 450, 600, 900, 1,800, 3,600, and 5,400 (for ^{18}F-**AMC20**) seconds after tracer injection.

After aliquots of intact blood were withdrawn, samples were centrifuged to obtain plasma. Radioactivity of plasma and intact blood aliquots was measured with a γ counter. Radiometabolite content in the deproteinated plasma was assessed by radio–thin-layer chromatography (radio-TLC). Detailed procedures of arterial blood and plasma workup are described in the supplemental materials.

After the end of the PET scans (98 ± 8 min after injection for ^{18}F-**AMC20**), anesthetized animals were sacrificed by heart extirpation and dissected. Samples of brain and peripheral tissues were taken. All samples were weighed, and their radioactivity was measured with a γ counter.

Small-Animal PET Data Analysis

List-mode data from the 106-min-long and 76-min-long scans were reframed into, respectively, 90-min-long and 60-min-long dynamic sequences of 6×10, 4×30, 2×60, 1×120, 1×180, 4×300, 3×600, and (for 90-min-long scans) 2×900 s frames. The data were reconstructed per time frame using an iterative reconstruction algorithm (attenuation-weighted 2-dimensional ordered-subset expectation maximization, provided by Siemens; 4 iterations, 16 subsets; zoom factor, 2). Datasets were fully corrected for random coincidences, scatter, and attenuation. Data from the transmission scan were used for attenuation correction. The final datasets consisted of 95 slices, with a slice thickness of 0.8 mm and an in-plane image matrix size of 128×128 and pixel size of 0.47×0.47 mm.

PET data were analyzed with the Inveon 3.0 software package (Siemens Medical Solutions, USA, Inc.). ROIs were drawn manually on a T2-weighted MR imaging template of rat brain around the striatum, brain stem, cortex, hippocampus, hypothalamus, thalamus, olfactory bulbs, and cerebellum; around the whole brain; and around the pituitary gland. The MR imaging template was coregistered with the PET scan by image fusion. The time–activity curves per ROI were determined in Bq/cm^3 and used in this form for kinetic analysis but converted into standardized uptake values for presentation purposes.

TABLE 1
Injected Doses and Pretreatment Timing

Tracer	Injected activity (MBq/rat)	Injected dose (nmol/kg)	Pretreatment time interval (min)
^{18}F-**AMC20**	6.3 ± 1.7	1.58 ± 1.00	32 ± 16
^{11}C-raclopride	16.9 ± 5.3	1.26 ± 0.16	36 ± 3

Kinetic analysis is described using the nomenclature proposed by Innis et al. (*17*). ROI time–activity curves were analyzed with 1-tissue and 2-tissue compartmental models (1TCM and 2TCM, respectively) of reversible binding and with Logan graphical analysis, using a metabolite-corrected plasma-derived arterial input function and whole blood time–activity curve. Fractional cerebral blood volume was defined as 3.6%. ROI time–activity curves were also analyzed with the simplified reference tissue model (SRTM), using the cerebellum as the reference region.

Distribution volumes (V_Ts) per ROI were determined from 1TCM- and 2TCM-derived rate constants and by Logan analysis.

Binding potentials (BP_{ND}s) per ROI relative to the cerebellum were calculated from the obtained V_T values as V_T (target)/V_T (cerebellum) – 1, or estimated directly with STRM.

Ex Vivo Autoradiography and Brain Radiometabolite Analysis

Anesthetized rats, pretreated with saline ($n = 3$) or raclopride ($n = 3$), were injected (30 ± 5 min after pretreatment) with a short bolus of ^{18}F-**AMC20** (3.8 ± 1.0 MBq, 0.75 ± 0.19 nmol/kg) into the penile vein. Rats were sacrificed by heart extirpation 35 min after injection. Brains were quickly extracted and separated into 2 halves along the sagittal symmetry plane or along the coronal plane spanning the thalamus.

One brain half was sliced on the microtome, and the slices containing the striatum were exposed against the phosphor storage screens. From the other half, radioactivity was extracted by homogenization in acetonitrile (>90% efficiency) and analyzed by radio-TLC. Detailed protocols for both procedures are presented in the supplemental materials.

Outcome Measures of $D_{2/3}$R-Specific Binding

$D_{2/3}$R-specific binding of ^{18}F-**AMC20** was quantified using BP_{ND} values (as described above) and specific binding ratios (SBRs), the latter calculated as target region activity/cerebellar activity – 1. Both were estimated under control conditions and under raclopride challenge conditions.

Statistics

All data are presented as mean ± SD. When a comparison of means was done, the 2-sided unpaired Welch *t* test was used. *P* values below 0.05 were considered significant. In the case of multiple comparisons, no correction of α levels was performed.

RESULTS

Pharmacology

Competition curves of ^{3}H-spiperone displacement from the Long isoform of D_2R (D_2RLong) by **AMC20** were significantly better fitted by the 2-site binding model (inhibition constant for the high-affinity state = 85 pM and inhibition constant for the low-affinity state = 84 nM, 988-fold difference) than by the 1-site binding model. The same was true for short isoform of D_2R and D_3R (Table 2). Such biphasic binding is a hallmark of an agonist, and the difference in the agonist affinities for the 2 recognized binding sites is known to correlate with the intrinsic activity (*18*). No second high-affinity binding component was detected for D_1R. The D_1R affinity of **AMC20** was an order of magnitude lower than the lowest affinity at a D_2-like receptor (Table 2).

The arrestin recruitment assay showed **AMC20** to be an almost full agonist (the maximum response achievable for the tested ligand [**AMC20**] relative to the maximum response achievable for dopamine, 90.3% ± 5.4%) with a decimal logarithm of the reciprocal of the ligand concentration (in mol/L) eliciting the response equal to the 50% of the maximum of 8.86 ± 0.05.

Radiochemistry

^{18}F-**AMC20** was synthesized within 150 min (including purification and quality control) using the 3-step 2-pot reductive amination procedure (Fig. 2) in a 24% ± 7% decay-corrected isolated radiochemical yield and greater than 95% radiochemical purity. The specific activity was 39 ± 23 GBq/μmol at the end of synthesis.

The LogD distribution coefficient (octanol/phosphate buffer pH 7.4) of ^{18}F-**AMC20** was found to be 2.33 ± 0.03.

In Vitro Autoradiography

In rat brain slices, ^{18}F-**AMC20** showed preferential uptake in the $D_{2/3}$R-rich striatum (Fig. 3A). At the lowest radioligand

TABLE 2
In Vitro Affinity of **AMC20** Toward Dopamine Receptor Subtypes

Ligand	D_1	D_2Long		K_iLow/K_iHigh	D_2Short		D_3	
		High	Low		High	Low	High	Low
AMC20	5,062	0.085	84	988	25	399	0.6	219
FBu-AMC13*	6,912	5.6	80.5	14.4	1.3	92.7	—†	12.1
AMC1*	7,253	2.98	70	23.5	40	736	—	3.2
(−)NPA*	—	0.075	1.73	23.1	0.1	10.6	—	1.91
(+)PHNO*	—	0.45	21.4	47.6	n.d.	19	—	1.08
Dopamine*	—	231	11,581	50	n.d.	920	—	24.8

*Data from van Wieringen et al. (*15*).
†No high-affinity component detected.
All values are mean K_i values (≥3 independent experiments) in nM.
K_iLow = inhibition constant for low-affinity state; K_iHigh = inhibition constant for high-affinity state.

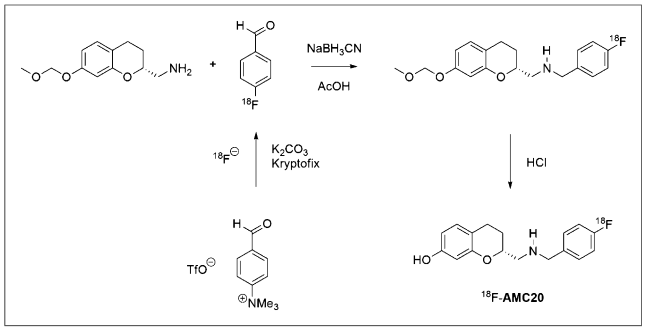

FIGURE 2. Radiosynthesis of ^{18}F-**AMC20**.

concentration tried (1.7 nM), striatal SBR of ^{18}F-**AMC20** was 5.27 ± 1.49 at baseline and 0.89 ± 0.29 (by 83%) in the presence of 10 μM raclopride, so 70% of the ^{18}F-**AMC20** binding in the striatum was $D_{2/3}$R-specific. In the concentration range of 1.7–7.8 nM, 10 μM raclopride decreased striatal SBR values by 74%–89%, compared with control conditions, whereas 100 μM GTP decreased the SBR by 62%–78%, implying that most of the $D_{2/3}$R-specific striatal binding of ^{18}F-**AMC20** was to the high-affinity subset of the receptors (Fig. 3B).

Uptake in Living Rat Brain Under Control Conditions

^{18}F-**AMC20** showed excellent blood–brain barrier penetration (Fig. 4): 3.5 min after injection, 1.7% injected dose (ID) accumulated in the brain.

The tracer primarily accumulated in the striatum, whereas the cerebellum showed the lowest uptake (Fig. 5A). The PET-derived striatum–to–cerebellum uptake ratio of ^{18}F-**AMC20** peaked 35 min after injection at 1.97 ± 0.13 (Fig. 5B). The same ratio for ^{11}C-raclopride 35 min after injection was 6.43 ± 0.89. The ex vivo autoradiography–derived striatum-to-cerebellum ratio of ^{18}F-**AMC20** at the same time after injection was 2.48 ± 0.34.

Ex vivo measurements of the ^{18}F-**AMC20** uptake in the brain and peripheral tissues performed after the PET scan are given in Supplemental Table 1.

Tracer Metabolism

^{18}F-**AMC20** was quickly metabolized and excreted from the plasma (Fig. 6). Plasma elimination half-life was 3.9 min. Radiometabolites found in the plasma and in the radioactivity extracted from the brain 35 min after injection showed R_f values of 0 in the radio-TLC analysis, compared with an R_f of 0.65 for ^{18}F-**AMC20.** Intact ^{18}F-**AMC20** constituted 95% of radioactivity from the above-mentioned brain tissue extract (Supplemental Fig. 2), suggesting that radiometabolites of ^{18}F-**AMC20** were hydrophilic and did not penetrate the blood–brain barrier.

In vivo defluorination was also low, as follows from the much lower tracer uptake in the parietal bone, compared with the brain tissue (Supplemental Table 1).

Kinetic Analysis

ROI time–activity curves of control rats were consistently better approximated by 2TCM and SRTM than by 1TCM (Supplemental Fig. 3), as assessed by the Akaike information criterion. However, no consistent estimates of individual rate constants could be obtained from 2TCM fits (Supplemental Table 2).

Logan graphical analysis produced the most robust ROI V_T estimates (Supplemental Table 3). 2TCM-derived V_T values correlated better with Logan V_T values (r = 0.98) than did 1TCM V_T values (r = 0.95; Supplemental Fig. 4). The 2TCM rate constant ratios k_3/k_4 did not provide robust BP_{ND} estimates (data not shown), but V_T-based 2TCM BP_{ND}s were robust and correlated better with Logan BP_{ND} values (r = 0.99) than did 1TCM BP_{ND} values (r = 0.93).

SRTM BP_{ND} values correlated best with Logan BP_{ND}s (r = 0.95), somewhat less well with 2TCM BP_{ND}s (r = 0.92), and still less well with 1TCM BP_{ND}s (r = 0.88; Supplemental Fig. 5).

The highest BP_{ND} values in saline-pretreated rats, 0.49–0.59 depending on the estimation method, were found in the striatum (Table 3; Supplemental Table 4).

Raclopride Challenge

Raclopride pretreatment resulted in a 35% decrease of peak PET-derived striatal SBRs of ^{18}F-**AMC20** relative to controls (0.63 ± 0.12 vs. 0.97 ± 0.13, $P < 0.01$). Blockade of $D_{2/3}$R-specific signal in the striatum was clearly seen on the ex vivo autoradiography images (Supplemental Fig. 6), and autoradiography-based SBR fell by 41% (0.88 ± 0.21 vs. 1.48 ± 0.34, $P < 0.01$).

Depending on the model used for kinetic analysis, striatal BP_{ND}s fell by 21%–29% ($P < 0.05$ for SRTM; $P < 0.07$ for Logan and 1TCM; $P = 0.09$ for 2TCM; Table 3; Supplemental Table 4).

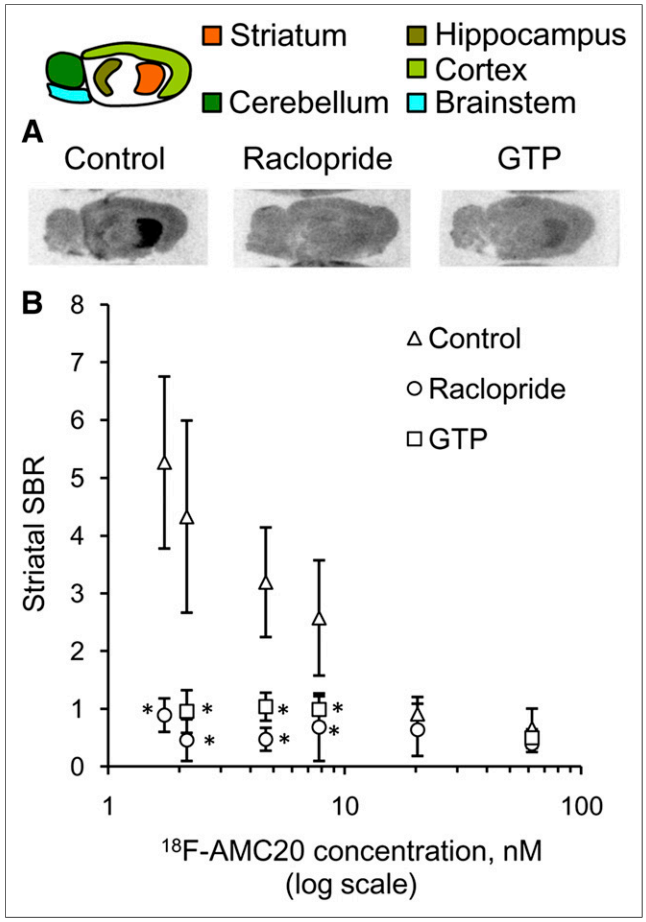

FIGURE 3. In vitro autoradiography assay results of ^{18}F-**AMC20.** Representative images (A) and influence of radioligand concentration on mean (±SD) striatal SBR of ^{18}F-**AMC20** (B) in control slices and in slices coincubated with raclopride (10 μM) or GTP (100 μM). *$P < 0.05$ relative to control values, 2-sided Welch test.

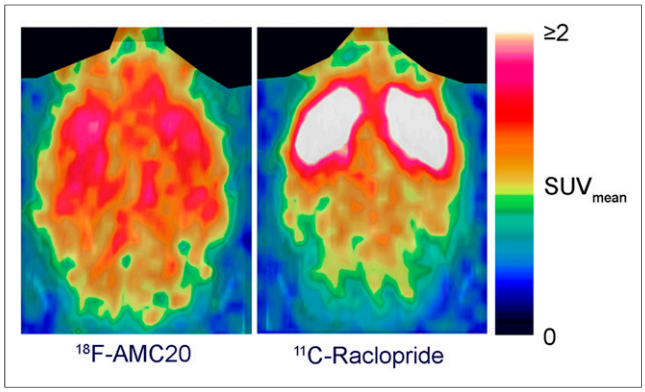

FIGURE 4. Representative in vivo PET images of ^{18}F-**AMC20** and ^{11}C-raclopride. Images are summed from 5 min after injection until end of scan. Harderian glands (on top) are masked. SUV_{mean} = mean standardized uptake value.

The occupancy of $D_{2/3}R$ by raclopride estimated from ROI V_T values with modified Lassen plot analysis (*19*) was found to be 34%–37% ($P < 0.05$ for 1TCM, 2TCM, and Logan). Comparison of the actual ROI V_T values with the estimated nondisplaceable volume of distribution implied that 39%–48% of striatal V_T and 5%–22% of cerebellar V_T were potentially displaceable (Supplemental Fig. 5).

DISCUSSION

This study is a continuation of our work on the development of $D_{2/3}R$ agonist PET tracers based on the AMC scaffold (*15,16*). Here we evaluated in vitro and in vivo a new candidate tracer, **AMC20.**

AMC20 was confirmed to be a potent D_2R agonist by the arrestin recruitment assay and demonstrated the highest D_2RHigh affinity (85 pM) and D_2RHigh/D_2RLow selectivity (988-fold) of all AMCs so far evaluated by us (Table 2). Likewise, in rat brain slices ^{18}F-**AMC20** exhibited high striatal SBRs and was as highly sensitive to the high-affinity state of $D_{2/3}R$-eliminating GTP as to the $D_{2/3}R$-blocker raclopride.

In living rats, ^{18}F-**AMC20** penetrated the blood–brain barrier well and preferentially accumulated in the striatum. The 2TCM model approximated the time–activity curves of ^{18}F-**AMC20** generally better than the 1TCM model, but there was no consistency in the estimates of individual rate constants of 2TCM. It may be that the data (i.e., PET counts and input curves) were not of sufficiently high quality to precisely estimate these constants. Still, the V_T values derived from the 2TCM rate constants, as well as V_T-based BP_{ND} values, were robust and consistent, so these outcome measures were used for the evaluation of ^{18}F-**AMC20.** Interestingly, both V_T and BP_{ND} obtained from 2TCM correlated better than V_T and BP_{ND} obtained from 1TCM with the corresponding measures obtained by Logan analysis, which does not assume any particular number of kinetic compartments.

Changes of striatal BP_{ND} and SBR induced by 1 mg of raclopride per kilogram were generally consistent with the estimates of $D_{2/3}R$ occupancy by raclopride but disagreed with the literature data for ^{11}C-labeled $D_{2/3}R$ agonists: as little as 0.2 mg/kg displaced over 80% of apparent $D_{2/3}R$-specific ^{11}C-(+)**PHNO** uptake (*20*), whereas 1–2 mg of raclopride per kilogram displaced more than 90% specific striatal uptake of ^{11}C-**MNPA** and ^{11}C-**PHNO** in Sprague–Dawley rats (*20–22*).

Crude estimation of the $D_{2/3}R$ occupancy by ^{18}F-**AMC20** in our experiments, assuming the equality of non–$D_{2/3}R$-specific binding in the striatum and cerebellum and using the approach described by Skinbjerg et al. (*23*), produced values ranging from 2% to 15% (7% on average). These values mean our injected tracer doses could have been high enough to cause a mass effect, distorting our measurements. However, baseline SBRs and BP_{ND}s of ^{18}F-**AMC20** in control rats did not tend to decrease with the injected dose (Supplemental Fig. 6), so we do not consider the violation of tracer conditions likely.

Imprecise estimation of the specific portion of total tracer binding, resulting from high nonspecific binding, may have led to the underestimation of the degree of specific binding blockade by raclopride. Low apparent displacement of $D_{2/3}R$-specific striatal binding may also suggest that in the brain ^{18}F-**AMC20** specifically binds to sites other than $D_{2/3}R$, which have comparatively high density in the striatum. Binding to D_1 has been ruled out in this study, whereas racemic **AMC20** was shown to be selective for D_2R against the serotonin-1A (5-hydroxytryptamine subtype 1A) and α_1 receptors (*14*), but selectivity against other nondopaminergic receptors has yet to be tested.

Compared with the earlier evaluated ^{18}F-**FEt-AMC13** (*16*), ^{18}F-**AMC20** showed greater decrease of striatal SBRs and BP_{ND} in response to raclopride treatment in living rats (Supplemental Table 5). However, ^{18}F-**AMC20** is inferior to existing ^{11}C-labeled $D_{2/3}$ agonists (*13,21,22*) in terms of baseline striatal BP_{ND} (0.49–0.59 vs. >0.8) and, apparently, also in terms of sensitivity to raclopride treatment.

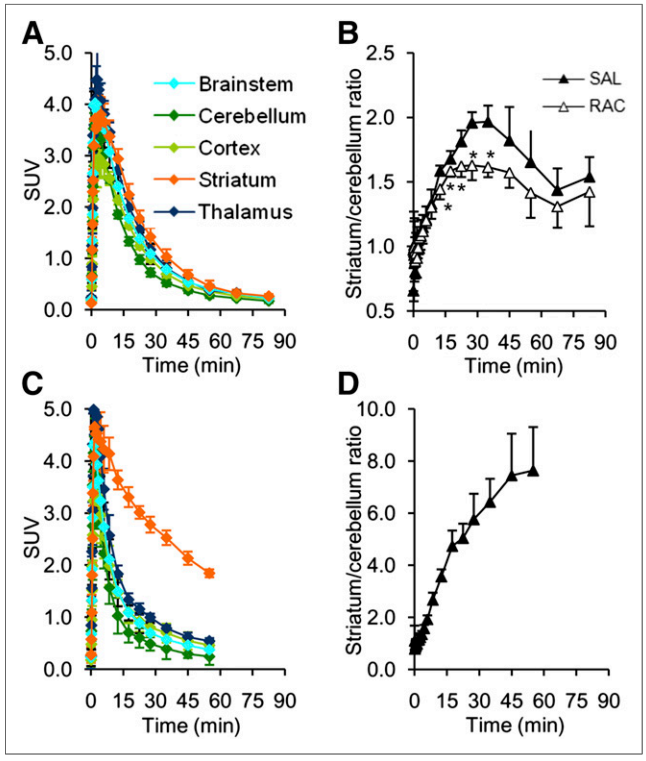

FIGURE 5. Uptake of ^{18}F-**AMC20** (A and B) and ^{11}C-raclopride (C and D) in rat brain. (A and C) ROI time–activity curves of control rats. (B and D) Striatum-to-cerebellum ratios in saline (SAL) and raclopride-pretreated (RAC) rats. Points represent group means; error bars show SD. *$P <$ 0.05 relative to control group, 2-tailed Welch *t* test. SUV = standardized uptake value.

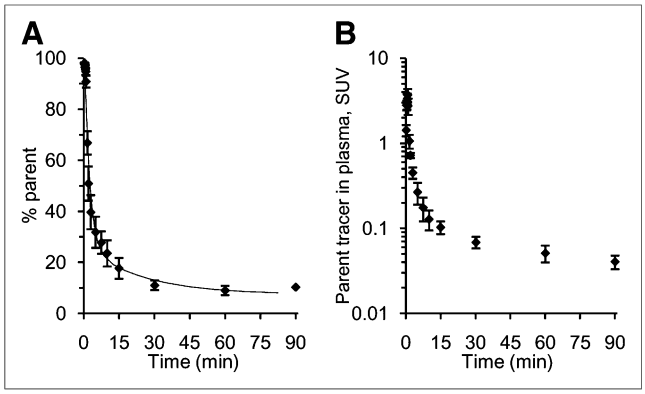

FIGURE 6. Metabolism and pharmacokinetics of ^{18}F-**AMC20** in plasma of living rats. (A) Percentage of parent in plasma radioactivity. (B) Intact ^{18}F-**AMC20** concentration in plasma. Points represent group means; error bars show SD. Horizontal axes show time after tracer injection. SUV = standardized uptake value.

The higher nonspecific binding of ^{18}F-**AMC20,** resulting from its considerably higher lipophilicity (LogD, 2.33 ± 0.03) relative to ^{18}F-**FEt-AMC13** (LogD, 1.67 ± 0.07), seems to have prevented ^{18}F-**AMC20** from attaining a high signal-to-noise ratio despite its high affinity toward $D_{2/3}$RHigh.

^{18}F-**AMC20** and ^{18}F-**FEt-AMC13,** both based on the **AMC1** structure, have, therefore, 2 common problems. One is the low signal-to-noise ratio, dependent on the association and dissociation rates of tracer binding to the receptors. Signal-to-noise ratio may be limited by the nonspecific binding of the tracer in the tissue, which leaves less free tracer available for specific binding, or by the quick release of specifically bound agonist tracer from the receptors due to the receptor's relaxation into the low-affinity state after G-protein activation by an agonist—a known potential issue for agonist tracers of G-protein–coupled receptors (*11*).

Another problem is the suspected lack of pharmacologic selectivity of ^{18}F-**AMC20** and ^{18}F-**FEt-AMC13** toward $D_{2/3}$R.

Screening of the **AMC20** and **FEt-AMC13** against nondopaminergic receptors and more thorough studies of their binding kinetics in a more controlled environment (in vitro) are necessary to find out which factors limit the signal-to-noise ratio of these compounds as $D_{2/3}$R imaging agents and to produce and evaluate new optimized AMC derivatives.

CONCLUSION

We have evaluated a novel aminomethyl chromane–derived $D_{2/3}$R agonist radiopharmaceutical. The agonist, **AMC20,** demonstrated high affinity toward the high-affinity state of human $D_{2/3}$RLong in cell membrane homogenates. ^{18}F-**AMC20** showed specific binding to the striatal $D_{2/3}$R in rat brain slices in vitro as well as in living rat brain. The signal-to-noise ratio of ^{18}F-**AMC20** was on a par with that of the structurally related tracer ^{18}F-**FEt-AMC13** evaluated by us earlier (*16*). Further investigations of the structure–activity relationships of ^{18}F-**AMC20** and related compounds can lead to a radioligand suitable for $D_{2/3}$R imaging in vivo.

DISCLOSURE

The costs of publication of this article were defrayed in part by the payment of page charges. Therefore, and solely to indicate this fact, this article is hereby marked "advertisement" in accordance with 18 USC section 1734. This work was supported by a grant from the Dutch Technology Foundation STW (grant 10127). No other potential conflict of interest relevant to this article was reported.

ACKNOWLEDGMENTS

We thank J.A.J.M. (Jef) Vekemans, Eindhoven University of Technology, (TU/e), for his advice on synthetic design; J.L.J. (Joost) van Dongen and R.A.A. (Ralf) Bovee (both TU/e) for their expertise on and execution of the HRMS measurements and the elemental analyses, respectively; E.W. (Bert) Meijer (TU/e and ICMS Eindhoven) for enabling the execution of the synthetic part of the presented research; and Aren van Waarde, Antoon Willemsen, Janine Doorduin, Jurgen Sijbesma, and Mohammed Khayum (all Department of Nuclear Medicine and Molecular Imaging, University Medical Center Groningen, University of Groningen) for their

TABLE 3
Logan- and SRTM-Derived BP_{ND} Values for ^{18}F-**AMC20**

ROI	Logan BP_{ND}		SRTM BP_{ND}	
	Control	Raclopride	Control	Raclopride
Striatum	0.49 ± 0.09	0.36 ± 0.07 (−26%)*	0.49 ± 0.08	0.35 ± 0.07 (–29%)†
Hippocampus	0.35 ± 0.06	0.35 ± 0.08 (0%)	0.37 ± 0.05	0.34 ± 0.09 (–6%)
Thalamus	0.39 ± 0.05	0.36 ± 0.09 (−10%)	0.39 ± 0.05	0.32 ± 0.07 (–19%)
Hypothalamus	0.20 ± 0.08	0.13 ± 0.05 (−35%)	0.14 ± 0.09	0.12 ± 0.05 (–14%)
Cortex	0.09 ± 0.03	0.11 ± 0.07 (22%)	0.08 ± 0.01	0.10 ± 0.06 (+18%)
Brain stem	0.29 ± 0.08	0.16 ± 0.04 (−43%)†	0.29 ± 0.08	0.14 ± 0.03 (–53%)†
Olfactory bulbs	0.06 ± 0.05	0.07 ± 0.10 (25%)	0.07 ± 0.05	0.07 ± 0.12 (+2%)
Pituitary	0.09 ± 0.11	0.06 ± 0.09 (−36%)	0.15 ± 0.13	0.07 ± 0.10 (–55%)

*$P < 0.07$, 2-sided Welch test.
†$P < 0.05$, 2-sided Welch test.
Data are mean ± SD (n = 4/treatment group). Change in BP_{ND} value after raclopride challenge relative to control group is shown in parentheses. 1TCM- and 2TCM-derived BP_{ND} values are presented in Supplemental Table 4.

advice on the design and help with the execution of the small-animal PET study.

REFERENCES

1. Howes OD, Kapur S. The dopamine hypothesis of schizophrenia: version III—the final common pathway. *Schizophr Bull.* 2009;35:549–562.
2. Booij J, Tissingh G, Winogrodzka A, van Royen EA. Imaging of the dopaminergic neurotransmission system using single-photon emission tomography and positron emission tomography in patients with parkinsonism. *Eur J Nucl Med.* 1999;26:171–182.
3. Volkow ND, Fowler JS, Wang G-J, Swanson JM. Dopamine in drug abuse and addiction: results from imaging studies and treatment implications. *Mol Psychiatry.* 2004;9:557–569.
4. Volkow ND, Fowler JS, Wang GJ, Baler R, Telang F. Imaging dopamine's role in drug abuse and addiction. *Neuropharmacology.* 2009;56:3–8.
5. Elsinga PH, Hatano K, Ishiwata K. PET tracers for imaging of the dopaminergic system. *Curr Med Chem.* 2006;13:2139–2153.
6. Chio CL, Lajiness ME, Huff RM. Activation of heterologously expressed D_3 dopamine receptors: comparison with D2 dopamine receptors. *Mol Pharmacol.* 1994;45:51–60.
7. Sibley DR, De Lean A, Creese I. Anterior pituitary dopamine receptors: demonstration of interconvertible high and low affinity states of the D-2 dopamine receptor. *J Biol Chem.* 1982;257:6351–6361.
8. Liu IS, George SR, Seeman P. The human dopamine D_2(Longer) receptor has a high-affinity state and inhibits adenylyl cyclase. *Brain Res Mol Brain Res.* 2000;77:281–284.
9. Narendran R, Mason NS, Laymon CM, et al. A comparative evaluation of the dopamine $D_{2/3}$ agonist radiotracer ^{11}C-(-)-*N*-propyl-norapomorphine and antagonist ^{11}C-raclopride to measure amphetamine-induced dopamine release in the human striatum. *J Pharmacol Exp Ther.* 2010;333:533–539.
10. Shotbolt P, Tziortzi AC, Searle GE, et al. Within-subject comparison of ^{11}C-(+)-PHNO and ^{11}C-raclopride sensitivity to acute amphetamine challenge in healthy humans. *J Cereb Blood Flow Metab.* 2012;32:127–136.
11. van Wieringen JP, Booij J, Shalgunov V, Elsinga P, Michel MC. Agonist high- and low-affinity states of dopamine D_2 receptors: methods of detection and clinical implications. *Naunyn Schmiedebergs Arch Pharmacol.* 2013;386:135–154.
12. Finnema SJ, Bang-Andersen B, Wikström HV, Halldin C. Current state of agonist radioligands for imaging of brain dopamine D_2/D_3 receptors in vivo with positron emission tomography. *Curr Top Med Chem.* 2010;10:1477–1498.
13. Finnema SJ, Stepanov V, Nakao R, et al. ^{18}F-MCL-524, an ^{18}F-labeled dopamine D_2 and D_3 receptor agonist sensitive to dopamine: a preliminary PET study. *J Nucl Med.* 2014;55:1164–1170.
14. Mewshaw RE, Kavanagh J, Stack G, et al. New generation dopaminergic agents. 1. Discovery of a novel scaffold which embraces the D2 agonist pharmacophore: structure-activity relationships of a series of 2-(aminomethyl)chromans. *J Med Chem.* 1997;40:4235–4256.
15. van Wieringen JP, Shalgunov V, Janssen HM, et al. Synthesis and characterization of a novel series of agonist compounds as potential radiopharmaceuticals for imaging dopamine $D_{2/3}$ receptors in their high-affinity state. *J Med Chem.* 2014;57:391–410.
16. Shalgunov V, van Wieringen J, Sijbesma J, et al. Evaluation of ^{18}F-AMC-15, ^{18}F-FPr-AMC-13 and ^{18}F-FEt-AMC-13 as candidate dopamine $D_{2/3}$-agonist radioligands for PET [abstract]. *J Nucl Med.* 2013;54(suppl 2):1108.
17. Innis RB, Cunningham VJ, Delforge J, et al. Consensus nomenclature for in vivo imaging of reversibly binding radioligands. *J Cereb Blood Flow Metab.* 2007;27:1533–1539.
18. Lahti RA, Figur LM, Piercey MF, Ruppel PL, Evans DL. Intrinsic activity determinations at the dopamine D_2 guanine nucleotide-binding protein-coupled receptor: utilization of receptor state binding affinities. *Mol Pharmacol.* 1992;42:432–438.
19. Cunningham VJ, Rabiner EA, Slifstein M, Laruelle M, Gunn RN. Measuring drug occupancy in the absence of a reference region: the Lassen plot re-visited. *J Cereb Blood Flow Metab.* 2010;30:46–50.
20. Wilson AA, McCormick P, Kapur S, et al. Radiosynthesis and evaluation of ^{11}C-(+)-4-propyl-3,4,4a,5,6,10b-hexahydro-2H-naphtho[1,2-b][1,4]oxazin-9-ol as a potential radiotracer for in vivo imaging of the dopamine D_2 high-affinity state with positron emission tomography. *J Med Chem.* 2005;48:4153–4160.
21. Seneca N, Zoghbi SS, Skinbjerg M, et al. Occupancy of dopamine D2/3 receptors in rat brain by endogenous dopamine measured with the agonist positron emission tomography radioligand ^{11}C-MNPA. *Synapse.* 2008;62:756–763.
22. Egerton A, Hirani E, Ahmad R, et al. Further evaluation of the carbon11-labeled $D_{2/3}$ agonist PET radiotracer PHNO: reproducibility in tracer characteristics and characterization of extrastriatal binding. *Synapse.* 2010;64:301–312.
23. Skinbjerg M, Seneca N, Liow J-S, et al. Dopamine beta-hydroxylase-deficient mice have normal densities of D_2 dopamine receptors in the high-affinity state based on in vivo PET imaging and in vitro radioligand binding. *Synapse.* 2010;64:699–703.